

## Ultrafast excited state deactivation of doped porous anodic alumina membranes

This article has been downloaded from IOPscience. Please scroll down to see the full text article.

2012 Nanotechnology 23 305705

(<http://iopscience.iop.org/0957-4484/23/30/305705>)

View [the table of contents for this issue](#), or go to the [journal homepage](#) for more

Download details:

IP Address: 14.139.223.67

The article was downloaded on 11/07/2012 at 03:59

Please note that [terms and conditions apply](#).

# Ultrafast excited state deactivation of doped porous anodic alumina membranes

Abhinandan Makhal<sup>1,3</sup>, Soumik Sarkar<sup>1,3</sup>, Samir Kumar Pal<sup>1</sup>,  
Hongdan Yan<sup>2</sup>, Dirk Wulferding<sup>2</sup>, Fatih Cetin<sup>2</sup> and Peter Lemmens<sup>2</sup>

<sup>1</sup> Department of Chemical, Biological and Macromolecular Sciences, S N Bose National Centre for Basic Sciences, Block JD, Sector III, Salt Lake, Kolkata 700 098, India

<sup>2</sup> Institute for Condensed Matter Physics, TU Braunschweig, Mendelssohnstraße 3, 38106 Braunschweig, Germany

E-mail: [skpal@bose.res.in](mailto:skpal@bose.res.in) and [p.lemmens@tu-bs.de](mailto:p.lemmens@tu-bs.de)

Received 26 March 2012, in final form 11 June 2012

Published 10 July 2012

Online at [stacks.iop.org/Nano/23/305705](http://stacks.iop.org/Nano/23/305705)

## Abstract

Free-standing, bi-directionally permeable and ultra-thin anodic aluminum oxide (AAO) membranes establish attractive templates (host) for the synthesis of nano-dots and rods of various materials (guest). This is due to their chemical and structural integrity and high periodicity on length scales of 5–150 nm which are often used to host photoactive nano-materials for various device applications including dye-sensitized solar cells. In the present study, AAO membranes are synthesized by using electrochemical methods and a detailed structural characterization using FEG-SEM, XRD and TGA confirms the porosity and purity of the material. Defect-mediated photoluminescence quenching of the porous AAO membrane in the presence of an electron accepting guest organic molecule (benzoquinone) is studied by means of steady-state and picosecond/femtosecond-resolved luminescence measurements. Using time-resolved luminescence transients, we have also revealed light harvesting of complexes of porous alumina impregnated with inorganic quantum dots (Maple Red) or gold nanowires. Both the Förster resonance energy transfer and the nano-surface energy transfer techniques are employed to examine the observed quenching behavior as a function of the characteristic donor–acceptor distances. The experimental results will find their relevance in light harvesting devices based on AAOs combined with other materials involving a decisive energy/charge transfer dynamics.

(Some figures may appear in colour only in the online journal)

## 1. Introduction

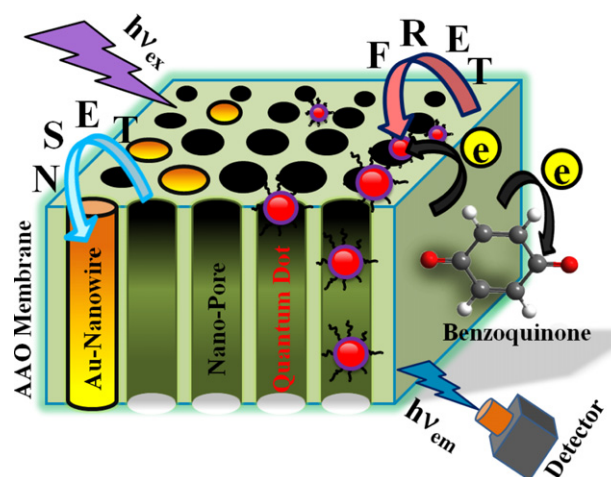
Anodic aluminum oxide (AAO) membranes prepared through a typical electrochemical procedure [1–3] possess highly-ordered nanopores with controllable and homogeneous dimensions arranged in a close-packed pattern [4]. The demonstrated dimensions of inter-pore spacing ranging from 50 to 400 nm and pore size from 25 to 300 nm are suitable for both quantum electronic effects and photonic crystals. Nowadays, AAO is an important material for a variety of nanotechnological applications because its unique nanoporous honeycomb structure can act as a template for

the fabrication of other nanostructured materials [5–11]. For example, AAO membranes are used as a template to grow different nanoscale materials like rare earth elements (Tb, Eu) [12, 13], polymers DBO-PPV (poly(2,5-dibutoxy-1,4-phenylenevinylene)) [14], MEH-PPV (poly(2-methoxy-5-(2-ethylhexyloxy)-1,4-phenylenevinylene)) [15], sensors [16], photonic crystals [17], energy storage and solar cells [18], magnetic storage devices [19], cell cultures [20] and drug delivery systems [21]. To enable studies of the interesting properties appearing for nanocomposites or nanodevices related to AAO films, a complete understanding of the self-properties of the AAO membranes is essential and necessary. Although many studies devoted to this topic have

<sup>3</sup> Both authors contributed equally.

been made, the origin of blue photoluminescence (PL) is controversially discussed. In general there are two main points of view to explain this phenomenon. The first one suggests that the observed blue emission band is caused by singly ionized oxygen vacancies ( $F^+$  centers) [22–24]. The other viewpoint is based on an assumption of Yamamoto *et al* [25] that oxalate impurities can be incorporated into the film during its formation which would transform into luminescent centers with the blue PL band around 470 nm. Using AAO membranes prepared in  $H_2SO_4$ , a similar PL phenomenon was observed by Du *et al*. Electron paramagnetic resonance measurements of the AAO membrane prepared in oxalic acid also reveal that the blue PL band arises from  $F^+$  centers [22, 24]. Therefore, it is already a well-accepted fact that the blue PL band of AAO arises from  $F^+$  centers. However, AAO membranes used in our experiment are annealed at  $500^\circ C$  to drive out any organic contaminants, mostly the oxalate impurities. Until now, most research works have focused on the magnetic and opto-electronic properties of nanoscopic materials and their fabrication mechanisms using AAO as a template material [26]. Recently, there has been growing interest in incorporating laser dyes into solid media for device applications, and some luminescent mechanisms have been discussed [27]. Jia *et al* have discussed the luminescence mechanisms of morin and morin–protein (trypsin and lysozyme) embedded into AAO films [28]. They have shown that the interaction of morin and the remaining aluminum in the AAO film and the coexistence of embedded dye and protein may be responsible for the PL appearance and enhancement, respectively.

In contrast to the previously reported studies, this work deals with the photo-induced charge transfer from electrochemically grown AAO membranes by anodizing aluminum in oxalic acid solutions and by studying their optical properties. Our aim is to establish the AAO membrane as an advantageous light harvesting material depicting both energy and electron transport ability in the presence of organic molecules and inorganic nanostructures. By using the femtosecond (fs)-resolved fluorescence upconversion technique, we have investigated charge transfer dynamics of AAO membranes in a complexation with benzoquinone (BQ) which is well known as an electron acceptor [29]. In this paper, we have explored the Förster resonance energy transfer (FRET) dynamics from AAO membranes to nanopore-embedded maple red (Map Red) QDs and gold nanowires (NWs). The use of FRET has been contemplated as an alternative mechanism for charge separation and a way to improve exciton harvesting [30]. In inorganic QD-based solar cells, the use of FRET to transfer the exciton generated in the QD to a high mobility conducting channel has been proposed as a way to bypass the traditional limitations of charge separation and transport [31, 32]. We report here on the use of FRET to boost the harvesting capacity of a light harvesting device. By using steady-state and picosecond (ps)-resolved fluorescence spectroscopy, we have demonstrated that defect-mediated PL from AAO membranes can be used to excite the guest QDs/Au NWs for the enhancement of light absorption possibility. In this



**Scheme 1.** Schematic illustration of the ultrafast excited state deactivation associated with both the electron and energy transfer reactions from the host porous AAO membrane to various guest organic molecules and inorganic nanostructures.

context, nano-surface energy transfer (NSET) [33], one of the other prevailing pathways of nonradiative quenching, is conclusively found to prevail in AAO–Au composites. A detailed demonstration of the ultrafast excited state deactivation of the porous AAO membrane in the presence of various fluorescence quenchers is schematically represented in scheme 1. This work may find its application to improve the efficiency of light harvesting devices.

## 2. Materials and methods

AAOs are prepared by a standard two-step anodization technique from high-purity (99.99%) aluminum foils of  $300\ \mu m$  thickness, developed by Masuda and co-workers [2]. Before anodization, the aluminum foils are annealed at  $400^\circ C$  for 3 h to relax grain-induced strain. Next the foils are electro-polished at 18 V for 4 min in a solution of mixed ethanol and  $HClO_4$  ( $CH_3CH_2OH : HClO_4 = 4:1\ v/v$ ). The first anodic oxidation process is performed in 0.3 M oxalic acid ( $C_2H_2O_4$ ) with an anodizing voltage of 50 V. After 8 h the alumina layer is removed by a mixed aqueous solution of 6%  $H_3PO_4$  and 1.8%  $H_2CrO_4$  at  $45^\circ C$  for 8 h. The second anodic oxidation process starts under the same conditions as the first one, with 8 h of oxidation time to grow the porous alumina layer with a thickness of around  $10\ \mu m$  on the Al foils. After that, a  $CuCl_2$  solution (6.8 g  $CuCl_2 + 100\ ml\ 37\%\ HCl + 200\ ml$  distilled water) is used to remove the Al foil on the back side of the AAO. After the sample becomes transparent, the additional barrier layer on the AAO is dissolved by a 5% phosphoric acid solution. The through-hole AAO is coated by a Ag film to be used as a cathode before depositing gold NWs (diameter = 45 nm) in the AAO matrix. Then the deposition process is performed in a solution of  $2.25 \times 10^{-3}\ mol\ l^{-1}\ HAuCl_4$  and  $0.485\ mol\ l^{-1}\ H_3BO_3$ , at a constant current of 0.04 mA. Maple Red orange (Map red) QD which is a suspension of CdSe QD with ZnS shell and TOP-TOPO capping was purchased from EVIDOTS, USA and benzoquinone (BQ) was obtained from Alfa Aesar.

For optical experiments, the steady-state absorption and emission are measured with a Shimadzu UV-2450 spectrophotometer and a Jobin Yvon Fluoromax-3 fluorimeter, respectively. Details of the ps-resolved spectroscopic data have been measured with a commercial time correlated single photon counting (TCSPC) setup from Edinburgh Instruments (instrument response function (IRF = 60 ps)), upon excitation at 375 nm. The ps-resolved decay curves are fitted by a nonlinear least square method to the tri-exponential decay law as given by the expression  $\sum_{i=1}^3 A_i \exp(-\frac{t}{\tau_i})$ , where  $A_i$  are weight percentages of the decay components with time constants of  $\tau_i$ . The average excited state lifetime is calculated by the relation ( $t = \frac{\sum_{i=1}^3 A_i \tau_i}{\sum_{i=1}^3 A_i}$ ) and  $\tau$  is used in FRET and NSET calculations in following sections.

Femtosecond-resolved fluorescence spectroscopy has been probed by a femtosecond upconversion setup (FOG 100, CDP) in which the sample is excited at 375 nm (0.5 nJ per pulse), using the second harmonic of a mode-locked Ti-sapphire laser with an 80 MHz repetition rate (Tsunami, Spectra Physics), pumped by a 10 W Millennia (Spectra Physics). The fundamental beam is frequency doubled in a nonlinear crystal (1 mm BBO ( $\beta$ -barium borate) crystal,  $\theta = 25^\circ$ ,  $\phi = 90^\circ$ ). The fluorescence emitted from the sample is upconverted in a nonlinear crystal (0.5 mm BBO,  $\theta = 10^\circ$ ,  $\phi = 90^\circ$ ) using a gate pulse of the fundamental beam. The upconverted light is dispersed in a double monochromator and detected using photon counting electronics. A cross-correlation function obtained using the Raman scattering from water displayed a full width at half maximum (FWHM) of 165 fs. The femtosecond fluorescence decays are fitted using a Gaussian shape for the exciting pulse.

The structural properties of the AAO membranes have been investigated using scanning electron microscopy (SEM, ZEISS SUPRA 35, EHT = 10 kV). Thermogravimetric analysis measurements (TGA, Perkin-Elmer TGA-50H) have been conducted with a sample weight of ca. 8 mg, a heating rate of  $10^\circ\text{C min}^{-1}$  and  $\text{N}_2$  as a carrier gas with a flow rate of  $20\text{ ml min}^{-1}$ .

In order to estimate FRET efficiency of the donor (AAO) and hence to determine distances of donor-acceptor pairs, we have used the following methodology [34]. The Förster distance ( $R_0$ ) is given by

$$R_0 = 0.211 \times [\kappa^2 n^{-4} Q_D J]^{1/6} \quad (1)$$

where  $\kappa^2$  is a factor describing the relative orientation in space of the transition dipoles of the donor and acceptor. For donor and acceptors that randomize by rotational diffusion prior to energy transfer, the magnitude of  $\kappa^2$  is assumed to be 2/3. The overall refractive index ( $n$ ) is considered to be 1.4. It has to be noted that on considering the refractive index of AAO medium to be 1.768 [35], the estimated donor-acceptor distances are found within 7% of the reported values. The integrated quantum yield of the donor ( $Q_D$ ) AAO in the absence of the acceptor is measured to be  $5.0 \times 10^{-3}$ , with respect to a reference dye Proflavine ( $Q_D = 0.34$ ).  $J$ , the overlap integral, which expresses the degree of spectral overlap between the

donor emission intensity (normalized to unit area) [36] and the acceptor absorption is given by

$$J = \frac{\int_0^\infty F_D(\lambda) \varepsilon_A(\lambda) \lambda^4 d\lambda}{\int_0^\infty F_D(\lambda) d\lambda} \quad (2)$$

where  $F_D(\lambda)$  is the fluorescence intensity of the donor in the wavelength range of  $\lambda$  to  $\lambda + d\lambda$  and is dimensionless.  $\varepsilon_A(\lambda)$  is the molar extinction coefficient (in  $\text{M}^{-1} \text{cm}^{-1}$ ) of the acceptor at  $\lambda$ . In this work, two energy-acceptor molecules have been studied, namely: Map Red QDs and Au NWs with extinction coefficients  $7 \times 10^5 \text{ M}^{-1} \text{cm}^{-1}$  ( $\lambda = 591 \text{ nm}$ ) [37] and  $7.66 \times 10^9 \text{ M}^{-1} \text{cm}^{-1}$  ( $\lambda = 528 \text{ nm}$ ) [38], respectively. If  $\lambda$  is in nm, then  $J$  is in units of  $\text{M}^{-1} \text{cm}^{-1} \text{nm}^4$ . The estimated values of the overlap integrals are  $1.57 \times 10^{17}$  and  $3.44 \times 10^{20} \text{ M}^{-1} \text{cm}^{-1} \text{nm}^4$  for Map Red and Au impregnated AAO, respectively. Once the value of  $R_0$  is known, the donor-acceptor (D-A) distance ( $r$ ) can be easily calculated using the formula

$$r^6 = \frac{[R_0^6(1 - E)]}{E} \quad (3)$$

where  $E$  is the efficiency of energy transfer which was measured using the relative fluorescence average lifetime of the donor, in the absence ( $\tau_D$ ) and the presence ( $\tau_{DA}$ ) of the acceptor.

$$E = 1 - \frac{\tau_{DA}}{\tau_D} \quad (4)$$

From the average lifetime calculation for the AAO-Map Red or AAO-Au adduct, we obtained the effective distances between the donor and the acceptor ( $r_{DA}$ ), using equations (3) and (4).

### 3. Results and discussion

A scanning electron micrograph of the side view of the porous alumina template is shown in figure 1(a), which reveals that the nanopores are uniform and highly ordered [39]. The inset (left side) shows the top view with  $\sim 48 \text{ nm}$  periodic pores separated by  $\sim 64 \text{ nm}$ . The pore diameter can easily be controlled by the anodization conditions, for example, the electrolyte type, concentration, applied voltage, and temperature. The thickness is adjusted by varying the time of the second anodization [6]. The right inset of figure 1(a) shows a cross view of Au wires in a typical sample. The length of these wires is controlled by the deposition time. Figure 1(b) shows the thermogravimetric analysis (TGA) of the as-prepared AAO where three weight loss regions are prominent, resembling the TGA curve reported by Sun *et al* [40]. The weight loss for the first section (room temperature  $-335^\circ\text{C}$ ) is mainly attributed to desorption of weakly bound water from the surface and inner walls of nanopores. In the second section ( $335-615^\circ\text{C}$ ), oxalate impurities are decomposed [41] and the third section ( $855-990^\circ\text{C}$ ) indicates a strong phase transition. Figure 1(c) shows the PL spectra (excitation at 375 nm) of the as-prepared AAO membranes along with AAO membranes annealed at

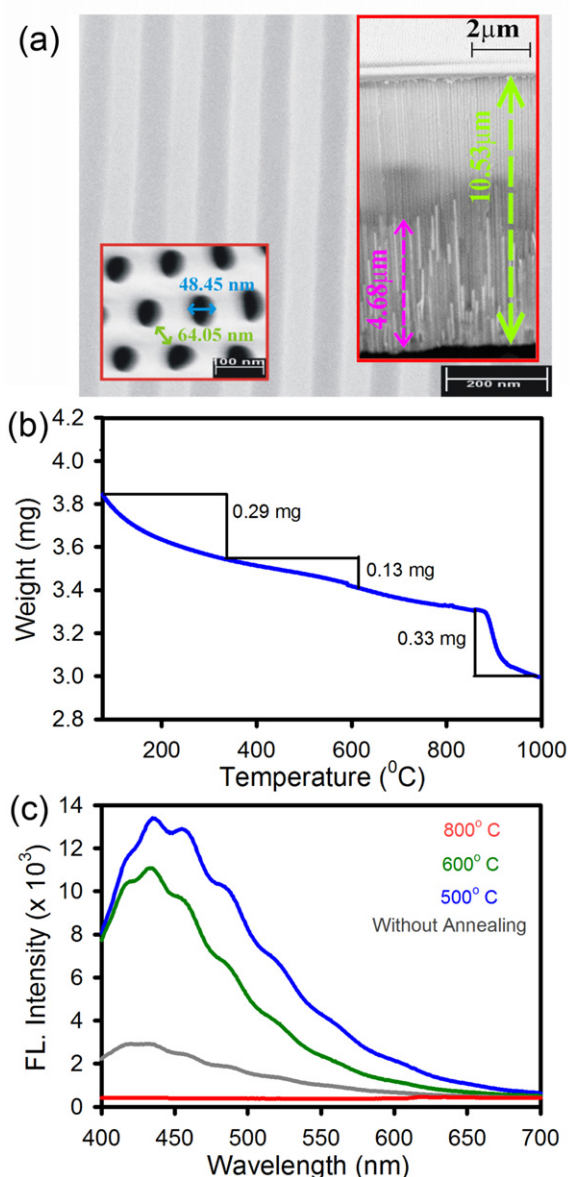


**Figure 1.** (a) Side view of AAO using electron microscopy showing uniform and highly-ordered nanopores. The left inset shows the top view with periodic pores. The right inset shows a side view of the Au wires in AAO. Different Au wire lengths at the edge are induced by breaking the sample for microscopy. (b) Thermogravimetric analysis curve for the as-prepared AAO membranes. (c) PL spectra of the as-anodized AAO and the AAO membranes annealed at different temperatures.

different temperatures. It is obvious that an intensive and broad PL emission band appears at about 450 nm [42] which originates from singly ionized oxygen vacancies ( $F^+$  centers) in AAO membranes [22]. The intensity of this band increases with elevated annealing temperature ( $T_a$ ) and reaches a maximum for the sample at  $T_a = 500^\circ\text{C}$ , but drastically decreases with a further increase in  $T_a$  [22, 40]. This phenomenon is well understood by considering the fact that during the heat treatment, oxygen in porous alumina membranes and oxygen diffusing from air into the membranes possibly react with the remaining aluminum in AAO, to form new alumina, and newly formed alumina may contain many

oxygen vacancies. With a further increase in the annealing temperature the PL intensity of AAO membranes becomes weak due to the fact that at very high temperatures the annihilation rate of oxygen vacancies becomes faster than the formation rate. The generation of new defect states upon air-annealing and the annihilation of defect states with increasing temperature are very common phenomena [22, 43]. Therefore, only a few  $F^+$  centers remain intact in porous alumina membranes, resulting in a sudden drop in the PL intensity. A similar broad green emission band at room temperature is also well known for ZnO NPs which has been studied in detail and demonstrated to originate from oxygen vacancy centers near the surface [44–46]. In particular, the origin of the blue–green emission peaking at 495 nm was demonstrated to be singly positive oxygen vacancy centers located at  $\sim 2$  nm from the surface of the ZnO nanoparticles [44–46]. In the present study, all optical experiments were carried out with the AAO membranes annealed at  $500^\circ\text{C}$  to obtain the maximum PL intensity and also to avoid any influence of organic contaminants, mostly the oxalate impurities. The emission bands and TGA analysis results obtained at different  $T_a$  thus confirm the purity of the AAO membranes used in our experiments.

We have investigated the defect-mediated blue band emission of AAO membranes in the absence and the presence of various emission quenchers impregnated in the AAO nanopores. Figure 2(a) represents the excitation spectra of bare AAO membranes and the room-temperature PL spectra of AAO. In order to investigate the electron transfer dynamics from the AAO membranes upon excitation, we have studied the complexation of the membrane with an organic molecule, benzoquinone (BQ), which is well known as an electron acceptor [29]. Infrared spectroscopic studies have shown that the carbonyl stretch vibration of the BQ is lowered in frequency as soon as the BQ adsorbs on the semiconductor surface [29]. The adsorbed BQ then acts as an electron acceptor and removes the photo-excited electron from the semiconductor conduction band in less time than the laser pulse duration ( $< 120$  fs) [45, 47, 48]. The steady-state and time (ps and fs)-resolved PL quenching (at 450 nm) of AAO upon complexation with BQ are shown in figures 2(a)–(c), respectively. The ps-resolved study on the AAO–BQ system exhibits timescales comparable to bare AAO, depicting the fact that the excited state electron transfer process must be too fast to be resolved in our ps-resolved luminescence study. Therefore, we have extended the study to the fs-timescale for a better understanding of the excited electron transfer process from AAO to the LUMO of BQ molecules. The sharp fluorescence decay (figure 2(c)) of AAO in the presence of BQ at the same excitation of 375 nm generates a new time constant of  $\sim 400$  fs (59%). Note that this short decay component is comparable to those reported for the CdSe–BQ adduct ( $\sim 600$  fs) which was demonstrated to arise due to electron transfer from the QD core to the surface attached BQ [48]. The resemblance of the electron transfer dynamics of BQ embedded AAO with those of the CdSe–BQ system clearly signifies the ultrafast photo-induced electron transfer dynamics from the host AAO to the organic guest molecule BQ.

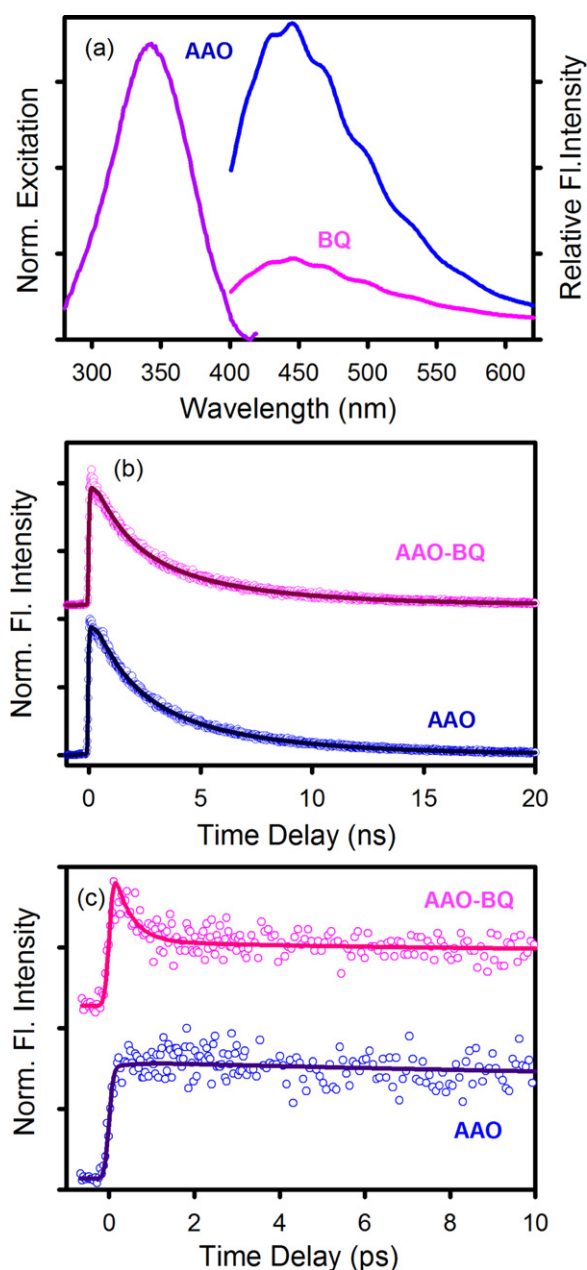


**Figure 2.** (a) Normalized excitation spectra and emission spectra of AAO membranes, in the absence and the presence of BQ. (b) The ps-resolved fluorescence transients of AAO membranes, in the absence (blue) and the presence of BQ (pink) (excitation at 375 nm) monitored at 450 nm. (c) The fs-resolved fluorescence transients of bare AAO (blue) and BQ impregnated AAO (pink) (excitation at 375 nm) collected at 450 nm showing faster decay.

As shown in figure 3(a), defect-mediated blue emission of bare AAO is noticeably quenched when it is impregnated with Map Red QDs or gold NWs. The ps-resolved faster excited state lifetimes of the AAO–Map Red and AAO–Au adducts with respect to that of the bare AAO are clearly noticeable from figure 3(b). Herein, we propose FRET from a donor AAO to Map Red or gold acceptors, which is responsible for the observed inhibition of emission bands. FRET in combination with Förster theory has become an invaluable tool for the assessment of distances in numerous biomolecular assemblies [34, 49, 50]. The FRET process

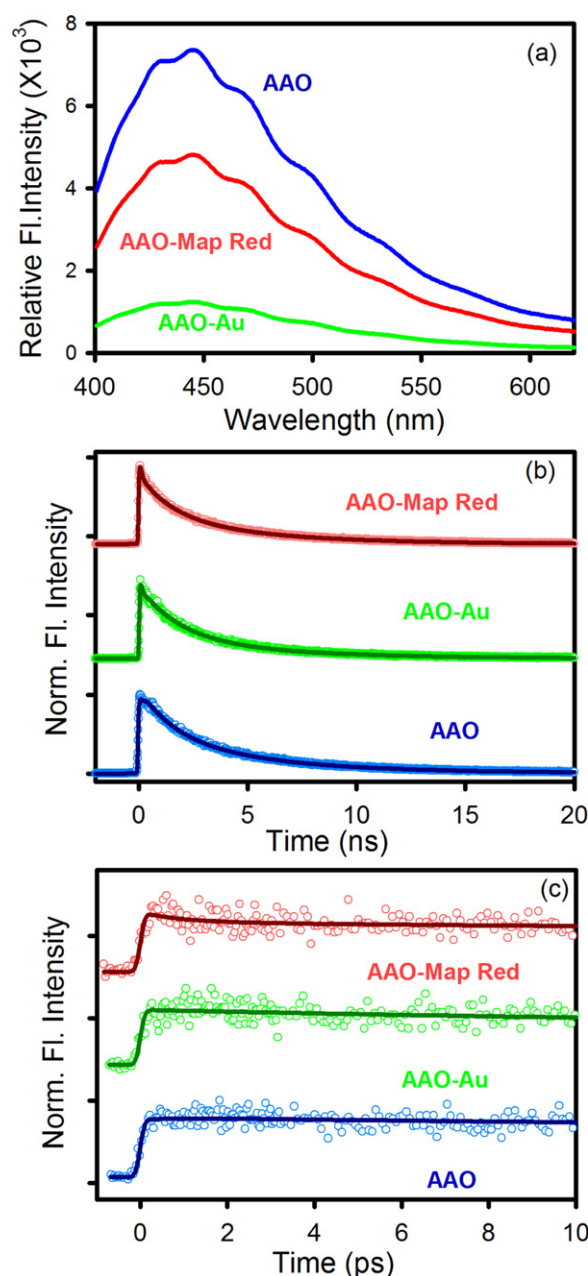


**Figure 3.** (a) Steady-state emission spectra of AAO membranes, in the absence and the presence of gold NWs and Map Red, (b) ps-resolved fluorescence transients (excitation at 375 nm, monitored at 450 nm) and (c) fs-resolved fluorescence transients of bare AAO (blue), Au NWs (green), and Map Red (red) impregnated AAO (excitation at 375 nm) collected at 450 nm.

is based on the concept of treating an excited donor as an oscillating dipole that can undergo energy exchange with a second dipole having a similar resonance frequency [34]. In principle, if the fluorescence emission spectrum of the donor overlaps the absorption spectrum of an acceptor, and the two are within a minimal distance from one another (1–10 nm), the donor can directly transfer its excitation energy to the acceptor via exchange of a virtual photon. The spectral overlap of the AAO emission spectrum with that of the Map Red and Au absorption spectrum is shown in figures 4(a) and (b), respectively. The details of the spectroscopic

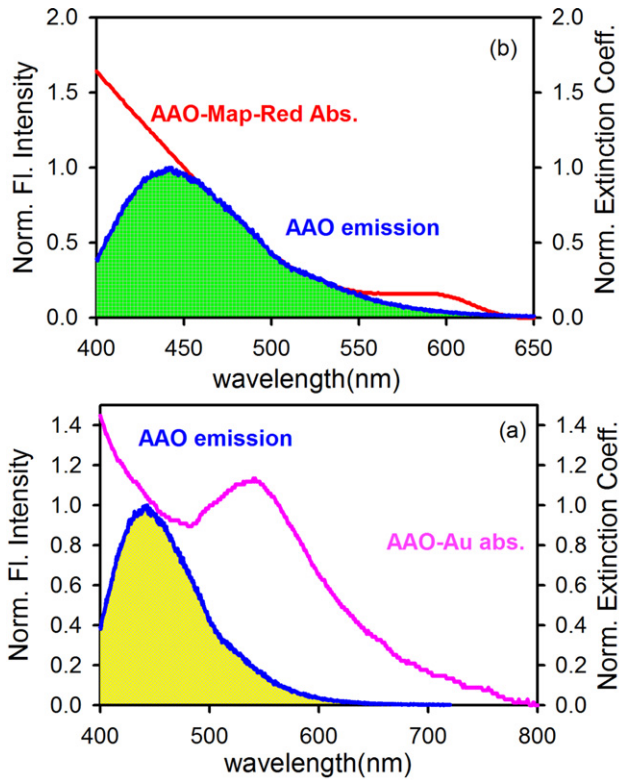


**Figure 4.** (a) Steady-state absorption spectra of acceptor Map Red (red) and emission spectra of donor AAO (blue) are shown. (b) Steady-state absorption spectra of acceptor gold NWs (red) and emission spectra of donor AAO (blue). The overlap zones are shown in green and yellow, respectively.

parameters and the fitting parameters of the luminescence transients are given in tables 1 and 2. From the average lifetime calculation (using equations (3) and (4)) for the AAO–Map Red and AAO–Au complexes, we obtain the effective distances between the donor and the acceptors,  $r_{DA} \approx 5.2$  nm and 21.5 nm, respectively. For AAO–QD complexation, the effective D–A distance is essentially the distance from donor singly positive oxygen vacancy states to the center of the acceptor QDs. However, the expected separation of the donor and the acceptor is supposed to be the radius of Map Red QDs ( $\sim 3.0$  nm, data not shown) [48]. By using FRET measurement on the AAO–QD system, we have estimated the D–A distance of 4.4 nm which reveals that the donor  $F^+$  centers are located within  $(5.2-3.0)$  nm = 2.2 nm from the AAO surface boundary. Note that the exact position of oxygen vacancy centers in AAO membrane is very much consistent with that in ZnO nanoparticles [44–46]. In contrast, by using the FRET technique, the D–A distance for the AAO–Au system is found to be 18.4 nm which is a larger value compared to the D–A distance between  $F^+$  centers and metal surface considering the fact that the donor  $F^+$  center transfers energy to the surface plasmon of the impregnated Au NWs, at the distance of  $\sim 2.2$  nm. The observation thus raises questions about the validity of FRET in the determination of the D–A distance in the case of the AAO–Au system.

The D–A separations can also be calculated using another prevailing technique, nano-surface energy transfer

**Table 1.** Picosecond-resolved luminescence transients of bare AAOs and AAOs in the presence of several quenchers. (Note: the emission from the AAO membrane (emission at 450 nm) was detected with 375 nm laser excitation. The numbers in parentheses indicate relative weights.)

Sample	$\tau_1$ (ns)	$\tau_2$ (ns)	$\tau_3$ (ns)	$\tau_{av}$ (ns)
AAO	1.47 (46%)	4.54 (48%)	10.5 (6%)	3.49
AAO–BQ	1.42 (49%)	4.54 (46%)	10.5 (5%)	3.30
AAO–Map Red	0.15 (38%)	1.7 (37%)	5.5 (25%)	2.06
AAO–Au	0.79 (37%)	2.9 (50%)	7.8 (13%)	2.76

**Table 2.** Femtosecond decay periods of luminescence measured with AAOs (bare) and AAOs in the presence of several quenchers. (Note: the emission from the AAO membrane (emission at 450 nm) was detected with 375 nm laser excitation. The numbers in parentheses indicate relative weights.)

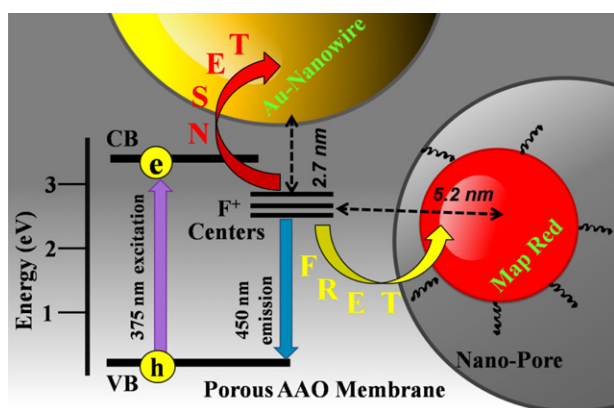
Sample	$\tau_1$ (ps)	$\tau_2$ (ps)	$\tau_3$ (ps) (fixed)
AAO	—	44.2 (28%)	1472 (72%)
AAO–BQ	0.40 (59%)	8.4 (6%)	1472 (35%)
AAO–Map Red	0.87 (17%)	12.2 (14%)	1472 (69%)
AAO–Au	—	35.5 (35%)	1472 (65%)

(NSET) [51, 52], in which the energy-transfer efficiency depends on the inverse of the fourth power of the donor–acceptor separation [53]. The NSET technique is based on the model of Persson and Lang [52], which is concerned with the momentum and energy conservation in the dipole-induced formation of electron–hole pairs. Here the rate of energy transfer is calculated by performing a Fermi golden rule calculation for an excited state material depopulating with the simultaneous scattering of an electron in the nearby metal to above the Fermi level. The Persson model states that the damping rate to a surface of a noble metal may be calculated by  $k_{NSET} = 0.3 \times (\frac{\mu^2 \omega}{\hbar \omega_F k_F d^4})$ , which can be expressed in more measurable parameters through the use of the Einstein  $A_{21}$  coefficient [54]  $A_{21} = \frac{\omega^3}{3\epsilon_0 \hbar \pi c^3} |\mu|^2$ .

To give the following rate of energy transfer in accordance with Coulomb’s law ( $1/4\pi\epsilon_0$ ):

$$k_{NSET} = 0.225 \frac{c^3 \Phi_D}{\omega^2 \omega_F k_F d^4 \tau_D}$$

where  $c$  is the speed of light,  $\Phi_D$  is the quantum yield of the donor (0.005),  $\omega$  is the angular frequency for the donor ( $4.2 \times 10^{15} \text{ s}^{-1}$ ),  $\omega_F$  is the angular frequency for bulk gold ( $8.4 \times 10^{15} \text{ s}^{-1}$ ),  $d$  is the donor–acceptor separation,  $\mu$  is the dipole moment,  $\tau_D$  is the average lifetime of the donor (3.48 ns), and  $k_F$  is the Fermi wavevector for bulk gold ( $1.2 \times 10^8 \text{ cm}^{-1}$ ) [55, 56]. In our case we used  $k_{NSET}$  as  $k_{NSET} = \frac{1}{\tau_{donor-acceptor}} - \frac{1}{\tau_{donor}}$ , where  $\tau_{donor-acceptor}$  is the average lifetime of the AAO–Au system. The calculated D–A distance using NSET is found to be 2.7 nm, which reflects the separation of donor  $F^+$  centers from the Au surface and also justifies the location of  $F^+$  centers from the AAO surface ( $\sim 2.2$  nm from surface boundary). A demonstration of the excited state energy transfer via the FRET and NSET mechanism is revealed in scheme 2 and effective D–A distances are shown in the presence of different acceptors.



**Scheme 2.** Schematic illustration of the FRET and NSET mechanism between donor  $F^+$  centers in the AAO membrane to the acceptors Map Red QDs and Au NWs showing their corresponding donor–acceptor distances.

Furthermore, it should be noted that fs-resolved luminescence transients (figure 3(c)) reveal a faster lifetime component of 0.87 ps which is associated with the excited state of the AAO–Map Red adduct and arises due to charge transfer from the AAO to the conduction band of the QDs. Therefore, it is clear that both the electron and energy transfer processes are coupled in the deactivation process of the excited AAO when it is embedded to Map Red QDs. However, no faster time constants are detectable from the fs-resolved luminescence transients of the AAO–Au composite, which suggests that the deactivation of AAO excited states occurs only via the NSET process.

#### 4. Conclusion

In summary, AAOs with an ordered pore size  $\sim 50$  nm were synthesized using electrochemical methods which provide a defect-mediated emission band near 450 nm. The present study provides a mechanistic explanation for the ultrafast excited state deactivation by considering every single aspect of the quenching mechanisms, namely charge transfer, Förster energy transfer and nano-surface energy transfer from the host AAO membrane to different guest molecules. The shorter lifetime as well as significant steady-state quenching was found when the AAO was impregnated with the well-known electron acceptor BQ, which accounted for fs-resolved charge transfer from the AAO conduction band to the BQ. We have also demonstrated that photo-excited AAO can transfer its energy to the impregnated QDs (Map Red) and Au NWs via FRET and NSET techniques, respectively. Based on these techniques, the location of the oxygen defect center is assigned and their distance from the surface adsorbed acceptor molecules is reported. Our present experiments and results will be beneficial to the understanding of the charge carrier or energy transfer processes from photo-excited AAOs to various acceptor molecules and it may find applications in the use of porous alumina in light harvesting devices.

#### Acknowledgments

AM thanks CSIR, and SS thanks UGC, India for their fellowships. We thank DST for a financial grant (SR/SO/BB-15/2007). HDY thanks IGSM. This work was partially supported by the NTH School, within the Project P1: ‘Energy conversion in molecular nano contacts’. We thank M Schilling and A Lak for important discussions.

#### References

- [1] Thompson G E, Furneaux R C, Wood G C, Richardson J A and Goode J S 1978 *Nature* **272** 433
- [2] Masuda H and Fukuda K 1995 *Science* **268** 1466
- [3] Masuda H, Hasegawa F and Ono S 1997 *J. Electrochem. Soc.* **144** L127
- [4] Ng C K Y and Ngan A H W 2011 *Chem. Mater.* **23** 5264
- [5] Zhang Y, Li G H, Wu Y C, Zhang B, Song W H and Zhang L 2002 *Adv. Mater.* **14** 1227
- [6] Chen D, Zhao W and Russell T P 2012 *ACS Nano* **6** 1479
- [7] Mei X, Kim D, Ruda H E and Guo Q X 2002 *Appl. Phys. Lett.* **81** 361
- [8] Hu W C, Gong D W, Chen Z, Yuan L M, Saito K, Grimes C A and Kichambare P 2001 *Appl. Phys. Lett.* **79** 3083
- [9] Sander M S, Prieto A L, Gronsky R, Sands T and Stacy A M 2002 *Adv. Mater.* **14** 665
- [10] Sander M S, Gronsky R, Sands T and Stacy A M 2003 *Chem. Mater.* **15** 335
- [11] Liu L, Lee W, Huang Z, Scholz R and Gösele U 2008 *Nanotechnology* **19** 335604
- [12] Pivin J C, Gaponenko N V, Molchan I, Kudrawiec R, Misiewicz J, Bryja L, Thompson G E and Skeldon P 2002 *J. Alloys. Compounds* **341** 272
- [13] Molchan I, Gaponenko N V, Kudrawiec R, Misiewicz J and Thompson G E 2003 *Mater. Sci. Eng. B* **105** 37
- [14] Zhao Y, Yang D, Zhaou C, Yang Q and Que D 2003 *J. Lumin.* **105** 57
- [15] Nguyena T P, Yanga S H, Rendua P L and Khan H 2005 *Composites A* **36** 515
- [16] Rumiche F, Wang H H, Hu W S, Indacochea J E and Wang M L 2008 *Sensors Actuators B* **134** 869
- [17] Masuda H, Ohya M, Asoh H, Nakao M, Nohtomi M and Tamamura T 1999 *Japan. J. Appl. Phys.* **38** L1403
- [18] Aguilera A, Jayaraman V, Sanagapalli S, Singh R S, Jayaraman V, Sampson K and Singh V P 2006 *Sol. Energy Mater. Sol. Cells* **90** 713
- [19] Nielsch K, Wehrspohn R B, Barthel J, Kirschner J, Gosele U, Fischer S F and Kronmüller H 2001 *Appl. Phys. Lett.* **79** 1360
- [20] Hua J, Tiana J H, Shia J, Zhanga F, Heb D L, Liuc L, Jungc D J, Baib J B and Chen Y 2011 *Microelectron. Eng.* **88** 1714
- [21] Simovic S, Losic D and Vasilev K 2010 *Chem. Commun.* **46** 1317
- [22] Du Y, Cai W L, Mo C M, Chen J, Zhang L D and Zhu X G 1999 *Appl. Phys. Lett.* **74** 2951
- [23] Li Y, Li G H, Meng G W, Zhang L D and Philipp F 2001 *J. Phys.:Condens. Matter* **13** 2691
- [24] Chen W, Tang H G, Shi C S, Deng J, Shi J Y, Zhou Y X, Xia S D, Wang Y X and Yin S T 1995 *Appl. Phys. Lett.* **67** 317
- [25] Yamamoto Y, Baba N and Tajima S 1981 *Nature* **289** 572
- [26] Martin C R 1994 *Science* **266** 1961
- [27] Shi G, Mo C M, Cai W L and Zhang L D 2000 *Solid State Commun.* **115** 253

- [28] Jia R, Shen Y, Luo H, Chen X, Hu Z and Xue D 2004 *Appl. Surface Sci.* **233** 343
- [29] Burda C, Green T C, Link S and El-Sayed M A 1999 *J. Phys. Chem. B* **103** 1783
- [30] Liu Y X, Summers M A, Scully S R and McGehee M D 2006 *J. Appl. Phys.* **99** 093521
- [31] Lu S and Madhukar A 2007 *Nano Lett.* **7** 3443
- [32] Yang Y, Rodríguez-Córdoba W, Xiang X and Lian T 2012 *Nano Lett.* **12** 303
- [33] Yun C S, Javier A, Jennings T, Fisher M, Hira S, Peterson S, Hopkins B, Reich N O and Strouse G F 2005 *J. Am. Chem. Soc.* **127** 3115
- [34] Lakowicz J R 1999 *Principles of Fluorescence Spectroscopy* (New York: Kluwer Academic/Plenum)
- [35] Apetz R and van Bruggen M P B 2003 *J. Am. Ceram. Soc.* **86** 480
- [36] Braslavsky S E, Fron E, Rodriguez H B, Roman E S, Scholes G D, Schweitzer G, Valeur B and Wirz J 2008 *Photochem. Photobiol. Sci.* **7** 1444
- [37] Yu W W, Qu L, Guo W and Peng X 2003 *Chem. Mater.* **15** 2854
- [38] Jain P K, Lee K S, El-Sayed I H and El-Sayed M A 2006 *J. Phys. Chem. B* **110** 7238
- [39] Yan H D, Lemmens P, Ahrens J, Bröring M, Burger S, Daum W, Lilienkamp G, Korte S, Lak A and Schilling M 2012 *Acta Phys. Sin.* at press
- [40] Sun X, Xu F, Li Z and Zhang W 2006 *J. Lumin.* **121** 588
- [41] Dollimore D 1987 *Thermochim. Acta* **117** 331
- [42] Huang G S, Wu X L, Mei Y F, Shao X F and Siu G G 2003 *J. Appl. Phys.* **93** 582
- [43] Djurišić A B et al 2007 *Nanotechnology* **18** 095702
- [44] Makhal A, Sarkar S, Bora T, Baruah S, Dutta J, Raychaudhuri A K and Pal S K 2010 *Nanotechnology* **21** 265703
- [45] Makhal A, Sarkar S, Bora T, Baruah S, Dutta J, Raychaudhuri A K and Pal S K 2010 *J. Phys. Chem. C* **114** 10390
- [46] Sarkar S, Makhal A, Bora T, Baruah S, Dutta J and Pal S K 2011 *Phys. Chem. Chem. Phys.* **13** 12488
- [47] Lou Y, Chen X, Samia A C and Burda C 2003 *J. Phys. Chem. B* **107** 12431
- [48] Makhal A, Yan H, Lemmens P and Pal S K 2010 *J. Phys. Chem. C* **114** 627
- [49] Clegg R M 1992 *Methods Enzymol.* **211** 353
- [50] Lilley D M J and Wilson T J 2000 *Curr. Opin. Chem. Biol.* **4** 507
- [51] Montalti M, Zaccheroni N, Prodi L, O'Reilly N and James S L 2007 *J. Am. Chem. Soc.* **129** 2418
- [52] Persson B N J and Lang N D 1982 *Phys. Rev. B* **26** 5409
- [53] Gersten J and Nitzan A 1981 *J. Chem. Phys.* **75** 1139
- [54] Craig D and Thirunamachandran T (ed) 1984 *Molecular Quantum Electrodynamics* (London: Academic)
- [55] Jennings T L, Singh M P and Strouse G F 2006 *J. Am. Chem. Soc.* **128** 5462
- [56] Muhammed M A H, Shaw A K, Pal S K and Pradeep T 2008 *J. Phys. Chem. C* **112** 14324